Journal of Fluids and Structures (2000) **14,** 1101–1117
doi:10.1006/jfls.2000.0318, available online at http://www.idealibrary.com on IDEAL®

HYDRODYNAMIC DAMPING OF A CYLINDER AT $\beta \approx 10^6$

J. R. CHAPLIN

Department of Civil and Environmental Engineering, University of Southampton Southampton, SO17 1BJ, U.K.

(Received 9 February 2000, and in final form 6 June 2000)

This paper describes delicate, but large-scale, experiments aimed at measuring the hydrodynamic damping of a circular cylinder oscillating in still water and transversely in a current. Attention is concentrated on the regime of very small Keulegan–Carpenter numbers, in which the drag coefficient is inversely proportional to the Keulegan–Carpenter number. Measurements in still water at $\beta = 650\,000$ and $1\,250\,000$ point to drag coefficients about twice those appropriate to two-dimensional laminar flow, in common with earlier measurements at $\beta \approx 10^5$. In the presence of a slowly varying transverse current (generated by placing the cylinder at the node of standing waves of long period), the damping increased with the reduced velocity of the ambient flow at a rate that increased with the Reynolds number.

1. INTRODUCTION

HYDRODYNAMIC DAMPING is important in predictions of the springing and ringing response of compliant systems such as Tension Leg Platforms. Considerable effort has been directed at developing an understanding of linear and nonlinear excitation in these cases, but much less attention has been given to the equally important question of the damping at the low Keulegan–Carpenter numbers of interest. Submerged components of TLPs have typical dimensions d of order 10 m, and their periods T of high-frequency oscillation (in pitch, roll and heave) are around 3 s. These figures indicate values of the Stokes parameter $\beta = d^2/\nu T$ of order 3×10^7. Typical amplitudes a of springing and ringing response are measured in centimetres, indicating Keulegan–Carpenter numbers $K = 2\pi a/d$ in the region of 0·01.

The problem of a cylinder undergoing harmonic oscillation in a direction normal to its axis with a small amplitude in a fluid otherwise at rest is also of classical interest. A solution for the case of two-dimensional attached laminar flow by Stokes (1851) was later extended by Wang (1968). If the instantaneous force acting on the cylinder per unit length is expressed as $C_d \frac{1}{2} \rho V |V| d$, where V is its velocity, then according to Wang's theory the drag coefficient is given by

$$C_d = \frac{3\pi^3}{2K}\left[(\pi\beta)^{-1/2} + (\pi\beta)^{-1} - \frac{1}{4}(\pi\beta)^{-3/2} + \cdots\right]. \tag{1}$$

At large β, equation (1) is closely approximated by

$$C_d = \frac{26{\cdot}24}{\sqrt{\beta}\,K}. \tag{2}$$

0889–9746/00/111101 + 17 $35.00/0

The use of a drag coefficient in this context may be misleading. It suggests that the relationship between the force and the velocity is nonlinear, whereas the theory predicts a force which is proportional to the instantaneous velocity. However, it has become customary to express damping in terms of a drag coefficient as in equation (1), casting the theoretical results in this form by means of the approximation $\cos\theta\,|\cos\theta| \approx (8/3\pi)\cos\theta$ [see, e.g., Bearman *et al.* (1985)]. Not much is known about the range of validity of equation (1), and some of the experimental evidence is contradictory. In experiments at $\beta = 1035$ and 1380, Sarpkaya (1986) found it in excellent agreement with measurements up to certain Keulegan–Carpenter numbers at which there was a step increase in C_d, followed by a second regime in which initially C_d was again inversely proportional to K. The critical Keulegan–Carpenter number corresponding to the step change in each case was in reasonable agreement with the prediction by Hall (1984) for the onset of the instability previously identified by Honji (1981). This consists of a series of mushroom-shaped vortex structures that propagate away from the cylinder on each side, with their axes in the plane of the oscillatory motion. According to Hall's analysis, the critical Keulegan–Carpenter number is given by

$$K_{\mathrm{cr}} = \frac{5{\cdot}78}{\beta^{1/4}}\left(1 + \frac{0{\cdot}21}{\beta^{1/4}} + \cdots\right). \tag{3}$$

At $\beta = 10^6$, this implies a threshold Keulegan–Carpenter number of 0·184.

Besides Sarpkaya (1986), who made measurements in the range $1035 < \beta < 11\,240$, comparable experimental studies of hydrodynamic damping (or of the drag coefficient) of a cylinder oscillating at small amplitudes in still water have been made by Otter (1990) ($\beta = 61\,400$), Troesch & Kim (1991) ($\beta = 23\,200$ and $48\,600$), Bearman & Russell (1996) ($\beta < 60\,000$), and Chaplin & Subbiah (1998) ($\beta < 166\,900$). In all cases in the present range of interest, the drag coefficient was predominantly inversely proportional to the Keulegan–Carpenter number, as in the theory, but the measured drag coefficients exceeded that predicted by equation (1) by ratios of between 1 (Otter) and 4·5 (Troesch & Kim). [In an earlier paper (Chaplin & Subbiah 1998), we erroneously cited in this context a ratio of about 5 observed by Sarpkaya at $\beta = 11\,240$]. This was based on measurements at $K > K_{\mathrm{er}}$ and therefore not relevant to this discussion. Sarpkaya did not report measurements for $K < K_{\mathrm{cr}}$ at $\beta = 11\,240$. Bearman & Russell and Chaplin & Subbiah found the ratio to be about 2 and 2·2, respectively, and it is worth noting that their experimental techniques were different both from each other, and from those employed earlier. Bearman & Russell suspended a vertical cylinder from a pendulum in a tank of water and observed its decaying oscillations following an initial displacement. In the experiments by Chaplin & Subbiah, a deeply submerged horizontal cylinder was mounted on springs and by means of an active control system subjected to an externally applied oscillating force at the resonant frequency. This had features in common with Troesch & Kim's and Otter's approaches, but was different from that followed by Sarpkaya, who measured forces on a stationary cylinder in oscillating flow.

The effects of vortex shedding also generate damping, and Bearman *et al.* (1985) predicted that the resulting contribution to the drag coefficient would be $0{\cdot}08\,K$, and this was subsequently found to be in good agreement with the measurements of Bearman & Russell. These, and the measurements of Chaplin & Subbiah, point to a semi-empirical formula for the total drag coefficient of the form

$$C_d = \frac{55}{\sqrt{\beta}\,K} + 0{\cdot}08\,K \tag{4}$$

(multiplying the Stokes result by a factor of about 2·1), for $20\,000 < \beta < 166\,900$.

For the case of hydrodynamic damping of a cylinder oscillating transversely in a steady current U (where the directions of the current, the cylinder axis, and the cylinder oscillations are all mutually perpendicular), there is still less information in the literature. In these conditions there is an additional parameter, the reduced velocity $U_r = U/fd$, where f is the oscillation frequency. A representative value of U_r for the case of a TLP (with current speeds of around 1 m/s) is 0·3, well below the range of conditions that have been studied in the context of locked-on vortex shedding.

The aim of the work described here was to extend the range of measurements of hydrodynamic damping of a cylinder to values of β closer to field conditions that had been previously achieved. Attention was directed at the limiting case of very small Keulegan–Carpenter numbers, below the theoretical instability threshold (3), for cases when the cylinder was oscillating in still water, and transversely in a current. Under these conditions, hydrodynamic damping can be expected to be very light; at $\beta = 10^6$ it is likely to be of a similar magnitude to the material damping in a steel structure. Therefore, considerable care was required in the design and construction of the experiment to ensure that such small levels of damping could be measured reliably. The practical arrangements are described in Section 2, and Section 3 reviews the most important issues concerned with the data processing. The results are discussed and summarized in Sections 4 and 5.

2. EXPERIMENTAL ARRANGEMENTS

The experiments were carried out in the Delta Flume at Delft Hydraulics. This flume is 230 m long, 5 m wide and 7 m deep, and has a solid beach with a compound slope. It is equipped with a carriage beneath which a rig was constructed for the present experiments, as shown in Figures 1 and 2. The apparatus consisted of a frame at each side of the flume, constructed from welded and bolted hollow steel box sections of cross-sectional dimensions 200 mm square and 10 mm wall-thickness. The test-cylinder, suspended elastically from the frames, was 0·75 m in diameter and 4·29 m long, fabricated from 12 mm thick steel. It had internal diaphragms to provide a central airtight section of length 3·47 m, ensuring that when submerged it was very nearly neutrally buoyant. A fine adjustment of its submerged weight was provided by partly filling its end cavities, from the top, with stiff water-repelling foam shortly before the cylinder was installed. The end cavities were otherwise full of water and closed off with disks fitted flush with the ends of the cylinder. The total mass of the cylinder was 1179 kg, and its external surface had a smooth painted finish.

The cylinder spanned the width of the Delta Flume at an elevation of 3·6 m above the floor and 1·9 m below the water surface, and was mounted at each end on the mid-point of a horizontal beam of solid steel, of length 6 m and cross-section 150 mm (horizontal) by 25 mm (vertical). These lower beams (see Figures 1 and 2) ran parallel to the sides of the flume and were stiffly attached to the frames at their ends. Their flexibility at mid-span allowed the cylinder to move vertically without rotation or lateral displacement.

The experiment was designed to avoid as far as possible all sources of damping except that on the cylinder itself. The predominant contribution to unwanted damping was expected to be that associated with the flow around the submerged lower beams as they oscillated with cylinder. To eliminate this effect, the lower beams were placed inside ducts, formed by the horizontal members of the frames, which could be evacuated. The connection at each end of the cylinder to the lower beam consisted of a crank that passed vertically downwards through a hole in the bottom of the duct, around which a skirt extended down a further 75 mm. The ducts were sealed everywhere else, so that when air was pumped into them (through pipes installed inside the outer descenders) it emerged first at the edges of the

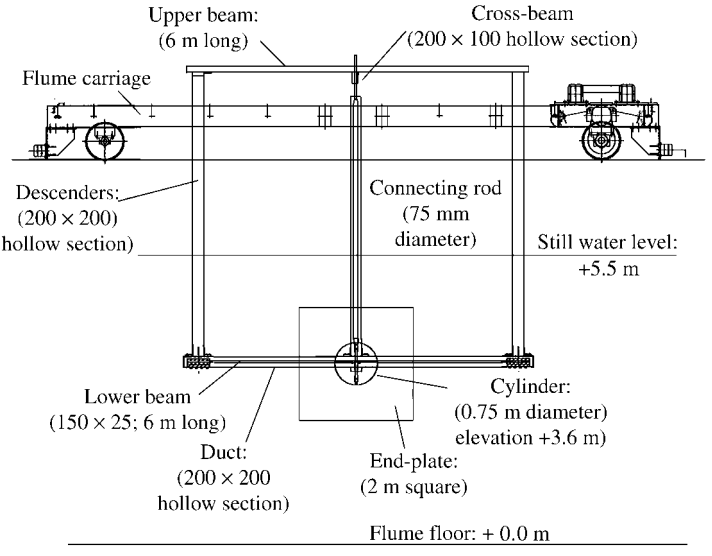

Figure 1. Elevation of the rig constructed beneath the carriage of the Delta Flume.

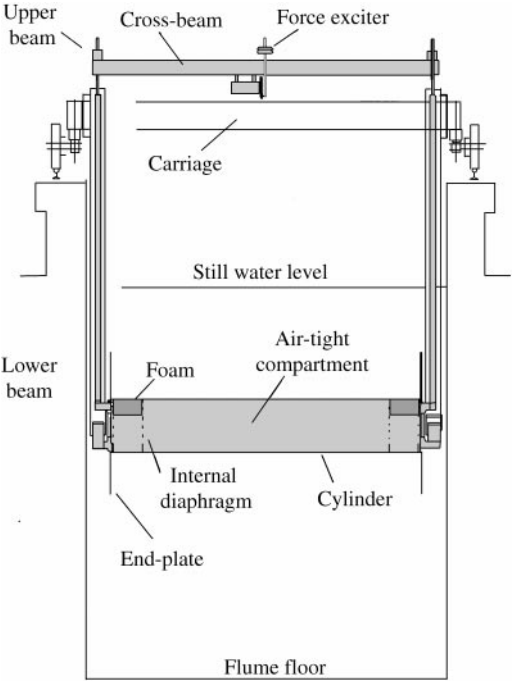

Figure 2. The cylinder and the cross-section of the rig in the Delta Flume. Components that oscillated with the cylinder are shaded.

skirts, by which time the beams were surrounded by air. A sketch of one of the lower beams in its duct is shown in Figure 3.

With this arrangement, measurements could be carried out either with the lower beams in water or in air. The latter was preferable and was used for most still water tests. In other

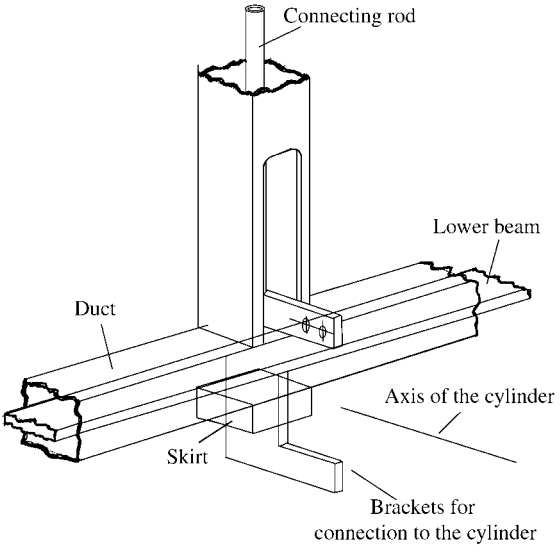

Figure 3. Sketch of the support system for the cylinder at one end.

conditions, however, (such as beneath the standing waves used in some tests described below), even with a constant flow of air into the ducts, changes in the ambient pressures would cause the water to flow in and out through the skirt, possibly impacting on the lower beams and generating additional hydrodynamic loading. For this reason, tests other than in still water were carried out with the ducts flooded, and that part of the measured damping that could be attributed to the submerged lower beams was subtracted from the result.

A second connection was made to each end of the cylinder, by a 75 mm diameter steel connecting rod that ran vertically up the central descender to emerge at the top. The upper ends of the connecting rods were attached to a second pair of beams, parallel with the lower ones, and of a similar length. These upper beams, which spanned between the tops of the outer descenders, could be changed to achieve different total stiffnesses, and therefore different natural frequencies of the cylinder. Two sets of upper beams were used in the experiments: solid steel flats of cross-section 150 mm (horizontal) by 40 mm (vertical), and secondly stainless steel box section of cross-sectional dimensions 80 mm square and 5 mm wall thickness. These beams produced natural frequencies respectively of 1·36 Hz and 2·08 Hz when the cylinder was submerged and the ducts were empty. By installing both sets of beams together, a third case was achieved with a submerged natural frequency of 2·30 Hz, and by inserting spacers between the beams, this was raised to 2·59 Hz. (The conditions are set out fully in Table 1 below.) Results are presented in this paper for cases 1 and 4; those for cases 2 and 3 have not been used here because (in case 2) there was an unidentified source of additional damping as described below, and (in case 3) there was clearly some damping associated with friction between the two pairs of upper beams.

The upper ends of the connecting rods were joined by a cross-beam (see Figure 2) on which was installed a variable-speed motor that drove a vertically oscillating bar, to which steel weights could be attached. This system provided a means of applying a vertical excitation to the cylinder and was used as a means of starting free decay tests, though this could also be done manually.

The vertical displacement of the cylinder was obtained from the output of strain gauges mounted on the lower beams. Four pairs of gauges were installed on each beam, with the

aim of identifying any departure from the first mode of oscillation of the beam. This was found to be negligible. Calibration of the gauges (and simultaneous measurement of the stiffness of the entire support system) was carried out in air and in still water by loading the cross-beam with concrete weights, and measuring its vertical displacement. An independent measurement of the cylinder movement was obtained from a nonintrusive Hamamatsu optical displacement transducer, positioned at the centre of the cross-beam.

End-plates made of marine ply, 2 m square, were positioned at each end of the cylinder as shown in Figure 2. They were not connected to the cylinder but rigidly attached to the framework alongside. In previous experiments (Bearman & Russell 1996; Chaplin & Subbiah 1998), end-plates were mounted on the cylinder, and the shear forces on them made a significant contribution to the total hydrodynamic damping. In order to identify the fluid forces acting on the cylinder alone, it had been necessary to repeat the measurements with cylinders of two different lengths, but with the same end-plates (the "long–short" method). Subsequently, experiments were carried out in the 55 m wave flame at City University, London, to explore the idea of mounting stationary end-plates at a small offset from the plane ends of the moving cylinder. As described in the Appendix, direct measurements of damping made in this way were found to be in good agreement with the earlier results for the damping on the cylinder alone. This approach was adopted for the Delta Flume experiments since it was much more efficient than repeating the tests with cylinders of different lengths. The gap between the stationary end-plates and the ends of the moving cylinder was about 10 mm. Slots in the end-plates accommodated connections between the ends of the cylinder and the lower beams and the connecting rods.

Other instruments included two electro-magnetic velocity meters positioned at one side of the flume and 6 m from the cylinder's axis towards the wavemaker. One was at the same elevation as the cylinder axis, and the other 0·5 m higher. Also, two wave-gauges measured the instantaneous water surface elevation, one directly above the cylinder, and the other on the same tank cross-section as the velocity meters.

3. THE MEASUREMENTS

3.1. Decay Tests

The cylinder's oscillations were started either manually or by switching the motor on and then off again after a few cycles of excitation at the cylinder's natural frequency. The amplitudes $a_1, a_2, \ldots, a_n, \ldots$ of the fundamental frequency component of each oscillation of the subsequent decaying motion were computed, and the sequence was fitted to a relationship which is a solution of

$$\frac{\partial K}{\partial n} = -2\pi(\zeta_0 + NK)\,K, \tag{5}$$

namely,

$$n = \frac{1}{2\pi\zeta_0} \ln\left[\frac{R(\zeta_0 + NK)}{K}\right], \tag{6}$$

where K is $2\pi a_n/d$, $\zeta = \zeta_0 + NK$ is the damping factor expressed as a proportion of critical damping, and R is a constant. The data were fitted to equation (6) by means of a standard curve-fitting routine, to yield values of ζ_0, N and R from each test.

Equation (5) is based on the observation that at small amplitudes the motion was dominated by viscous damping, but that initially the damping was amplitude-dependent. This was probably associated with transient that followed the artificial start, since the

Keulegan–Carpenter numbers were too small for vortex-shedding-induced damping (see above) to be significant. By fitting equation (5) to the data, the underlying viscous damping ζ_0 for a complete test could be found without the need for subjective decision about the time, during the decaying motion, beyond which other influences could be safely neglected.

Alternatively, ζ could be computed as a time series by numerical differentiation of the amplitude sequence in the usual way. In either case the drag coefficient was computed from

$$C_d = \frac{3\pi^3 m\zeta}{4MK}, \tag{7}$$

where m is the total oscillating mass (about 4000 kg including added mass) and M is the displaced mass of the cylinder (1895 kg).

3.2. Structural Damping

The structural damping for each condition was measured by carrying out decay tests in air, and this contribution was subtracted from measurements of the damping of the cylinder under water. When it was submerged, the whole cylinder assembly was neutrally buoyant, and the horizontal beams on which it was supported were very nearly straight. However, in air, the weight of the apparatus caused the beams to sag, giving rise to some additional stiffness associated with their elongation. The oscillating mass also was inevitably different from those of the underwater tests. The question then arises as to how the structural damping (predominantly due to internal damping in the steel beams) is changed by these factors. According to Lazan (1968, p. 62) under such conditions (in which a given member of a given material having linear-dashpot damping is loaded cyclically under different states of stress), the member loss modulus $k_s'' = c\omega$ is proportional to the member stiffness, where c is the damping force per unit velocity and $\omega = 2\pi f$ is the frequency of oscillation. This implies that under different states of loading, it is the damping factor $\zeta = c/2m\omega$ that is invariant. The present results were treated on this basis.

Measurements of free decay tests in air were fitted to equation (6) and the structural damping factor was taken to be the resulting value of ζ_0, minus a small correction for air resistance (less than 1%). A typical plot of decaying amplitudes of oscillation in air is shown in Figure 4, revealing excellent agreement with the form of equation (5). The structural damping of the cylinder under test conditions was close to 0.10%.

3.3. The Effect of Carriage Movement

During the initial tests it had become clear that the carriage did not provide a very rigid foundation for the oscillating rig. The carriage had a total mass of about 30 tonnes (8 tonnes of which was in the form of ballast over the rear driving wheels), and has a very stiff traction system. Nevertheless, vibration at the cylinder frequency could be detected in the structure of the carriage at several points, and was certainly contributing to the cylinder structural damping. This was about 0.2%, but rather variable, when the carriage was stationary, and still higher when it was driven along the flume at constant speeds. The situation was much improved by jacking the carriage up on to steel box-section struts 700 mm long, thereby transferring much of its weight directly to the top of the concrete sides of the flume. This had the effect of reducing the cylinder structural damping by about one-half, but of course removed the possibility of carrying out tests in currents simulated by towing the cylinder through still water. This was in any case problematic because at speeds of as little as 0·5 m/s there was sufficient excitation from the rails to promote an almost constant level of motion in the cylinder, at $K \approx 0{\cdot}007$.

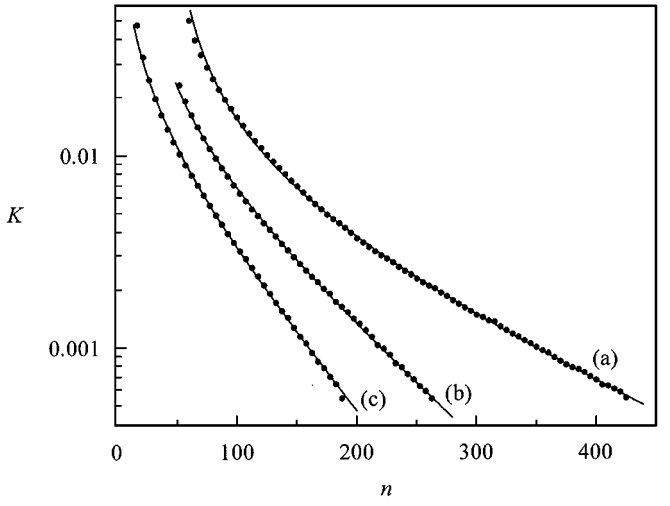

Figure 4. Results of free decay tests in case 4: (a) in air, $\zeta_0 = 0{\cdot}00111$, $N = 0{\cdot}149$; (b) in water with the ducts empty, $\zeta_0 = 0{\cdot}00212$, $N = 0{\cdot}144$; (c) in water with the ducts full, $\zeta_0 = 0{\cdot}00290$, $N = 0{\cdot}157$. The Keulegan–Carpenter numbers corresponding to the amplitude of every fifth cycle of oscillation (shown as points) are plotted against the cycle number, which is counted from an arbitrary zero. The lines represent equation (5) with the coefficients as shown.

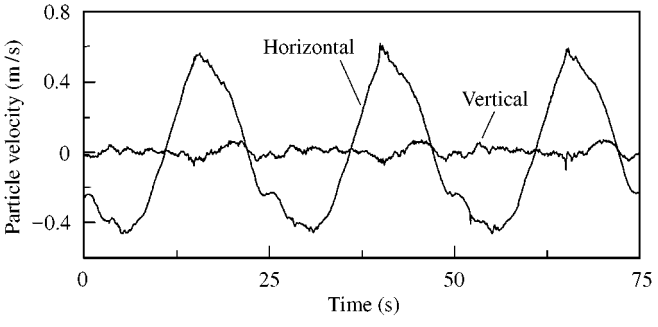

Figure 5. Particle velocities at the elevation of the cylinder, 6 m towards the waveboard, in standing waves of period 25 s, incident height 0.4 m.

As an alternative to producing the effects of a current by driving the carriage along the flume, experiments were carried out with the stiffly supported carriage positioned very close to the node of standing waves of period 25 s. The beach dissipated little of the wave energy at this frequency and a good-quality standing wave could be produced, as can be seen from the horizontal and vertical particle velocities plotted in Figure 5. In the largest waves, the horizontal and vertical excursions of a particle in the absence of the cylinder were calculated to be about 5 m and 0·3 m respectively, supporting the view that the ambient fluid motion around the cylinder was essentially a planar oscillatory flow with a very low frequency.

3.4. Effect of End Conditions

As mentioned above, the stationary end-plates were separated from the ends of the cylinder by small parallel gaps. Exploratory tests described in the Appendix had shown that this arrangement avoided the large-scale end-effects described by Bearman & Russell (1996), but it can be assumed that the ends of the cylinder would still experience an oscillating shear

stress, to which a first approximation can be provided by the solution (Stokes 1851) for a plate oscillating harmonically in its own plane. According to the theory (see the Appendix), the total damping force per unit velocity on two ends of the cylinder oscillating at frequency ω is $\frac{1}{2}\pi d^2\rho\sqrt{\omega\nu/2}$. Expressed as a drag coefficient for the whole cylinder, this corresponds to an increment

$$\Delta C_d = \frac{3\pi^3 d}{8LK}(\pi\beta)^{-1/2}, \tag{8}$$

where L is its length. In the present case, $\Delta C_d = 1{\cdot}15/(\sqrt{\beta}K)$, or about 2% of the viscous term in equation (4). This correction was applied to the results presented below.

3.5. Wavemaking Resistance

Oscillations of the cylinder inevitably generated waves at the surface, and though they could not be detected by eye it is worth checking whether the wavemaking resistance of the cylinder could make a significant contribution to the total damping. This can be done using the first-order solution for a horizontal cylinder beneath waves by Ogilvie (1963), from which (using Ogilvie's notation) it can be shown that the wavemaking damping force per unit velocity per unit length is

$$c_w = \frac{\pi\rho\omega d^2 S_\zeta \varepsilon_1}{4(1+S_\varepsilon^2)}, \tag{9}$$

regardless of the direction of oscillation. For the present conditions a solution of Ogilvie's theory for a frequency of 2 Hz gives $S_\zeta = 1{\cdot}2\times10^{-21}$, $\varepsilon_1 = 34{\cdot}8$, $S_\varepsilon = 1{\cdot}3\times10^{-16}$. The resulting value of c_w corresponds to a level of damping of about 10^{-22} % of critical. This was ignored throughout.

4. DISCUSSION OF RESULTS

4.1. Measurements in Air and in Still Water

For each case, the cylinder was oscillated in air and then in still water with the ducts in turn flooded and evacuated. The observed natural frequencies are given in Table 1, as are the stiffnesses that were measured statically as mentioned above. The reductions in natural frequencies caused by flooding the ducts are consistent with an increase in the oscillating mass in each case of about 250 kg, which is comparable with the total mass of water inside the ducts (310 kg), or the mass of water occupying a cylindrical volume surrounding the beams (210 kg).

Successive amplitudes of freely decaying oscillations observed in each case were fitted to equation (5), as shown in Figure 4. The results yielded values for the viscous part of the damping in each test, and these are set out in Table 2 as proportions of critical damping.

It is seen from Table 2 that in case 1 the structural damping measured in air was significantly higher than in cases 2 or 4, and it is argued that this can be attributed to the effects of buoyancy on the stiffness of the system. The final column of Table 2 shows stiffnesses inferred from the natural frequency in each case and the known total oscillating mass in air. That these are significantly higher (by 170%, 24% and 11%) than the stiffnesses that were measured when the cylinder was submerged (shown in column 4 of Table 1) is a result of the additional axial stiffness mentioned above, whose importance increases with the sag of the beams. Particularly in case 1 therefore, the oscillations in air — from which

TABLE 1
Experimental conditions, with natural frequencies measured in air and water

		In air		Under water			
				Ducts empty		Ducts full	
Case	Upper beams	Natural frequency	Stiffness (kN/m)	Natural frequency (Hz)	β	Natural frequency (Hz)	β
(1)	(2)	(3)	(4)	(5)	(6)	(7)	(8)
1	Solid steel flats: 150 mm by 30 mm	3·210	281	1·358	670 000	1·312	647 000
2	Stainless-steel box sections: 80 mm square 5 mm wall thickness	3·442	659	2·078	1 025 000	2·020	997 000
4	Both sets of beams, with steel spacers	3·949	1080	2·588	1 277 000	2·509	1 238 000

TABLE 2
Results of measurements of structural damping and of the damping associated with water inside the ducts. All the damping results are given as proportions of critical damping. The final column shows a natural frequency in air computed from the stiffness that was measured when the cylinder was submerged [given in column (4) of Table 1], and the mass of the cylinder and other oscillating components (but no added mass)

Case (1)	Structural damping (2)	Beam damping (3)	Inferred stiffness in air (kN/m) (4)
1	0·00139	0·00084	766
2	0·00103		817
4	0·00113	0·00079	1198

the structural damping was measured — took place in conditions that were dynamically very different from those of the cylinder when submerged. It seems reasonable to assume that this would render the measured structural damping of 0·00139 rather unrealiable (notwithstanding earlier discussion), and accordingly the structural damping in case 1 was subsequently taken to be midway between those of the other cases, namely 0·00108.

Though this adjustment in case 1 had a significant effect on the data (since the structural damping, beam damping, and cylinder damping were generally all of similar magnitudes—as can be seen in Figure 4), they are supported by the observation (see below) that the results for this case thus become compatible with those of the unaffected case 4 (at higher β), and those of Bearman & Russell (1996) and Chaplin & Subbiah (1998) (at lower β).

Measurements of the beam damping (shown in the third column of Table 2) were obtained from the differences between the damping observed in still water with the ducts in

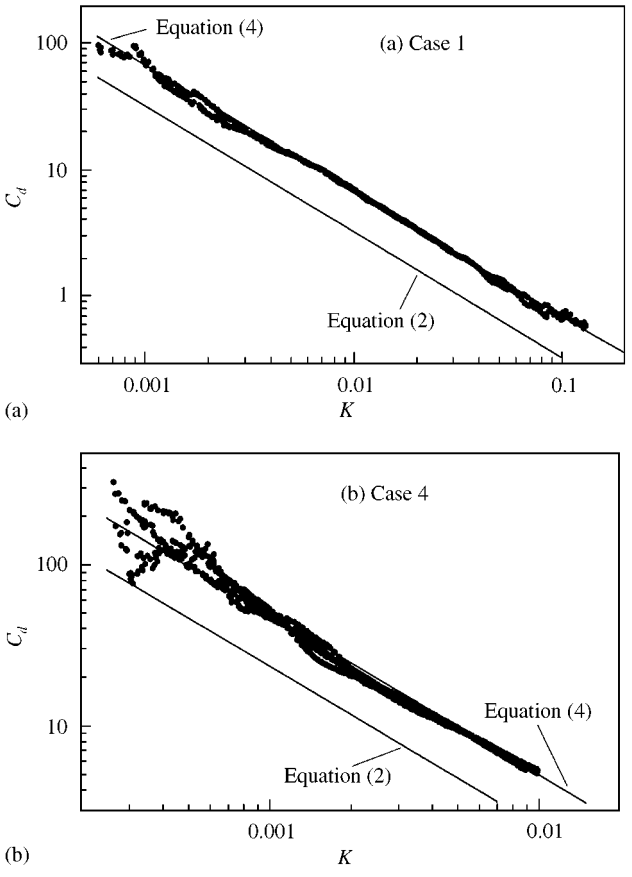

Figure 6. Drag coefficients in still water. The effects of structural damping have been subtracted, and equation (2) is the Stokes solution. In equation (4) drag coefficients from the Stokes solutions are multiplied by a factor of about 2·1. (a) Case 1, $\beta = 670\,000$; (b) case 4, $\beta = 1\,277\,000$.

turn evacuated and flooded, on the assumptions that the structural damping was constant, and that, over the resulting small reduction in frequency, the damping factor corresponding to the force on the cylinder was proportional to $\beta^{-1/2}$. In case 2 however, evacuating the ducts had very little effect on the measured damping, which remained close to that measured in cases 1 and 4 with the ducts full. No explanation was found for this behaviour; the case 2 tests were the first to be carried out, and it was not possible subsequently to study the motion of the rig under these conditions. Accordingly, for present purposes, the measurements in case 2 have been discarded, and the remainder of this paper is concerned only with the results of tests in cases 1 and 4. (However, if the same allowance is made for beam damping, measurements with the ducts flooded in case 2 were compatible with those of cases 1 and 4).

Drag coefficients obtained from decay tests in still water in cases 1 and 4, after correction for the effects of structural damping, are plotted in Figure 6, and compared with the results of equations (2) and (4). They are in good agreement with the latter, in common with the earlier results at lower β values. Overall drag coefficients corresponding to the values of ζ_0 in the curve-fit (5) appear in Table 3, where it can be seen that the measured hydrodynamic damping is almost exactly twice that predicted by Stokes theory (2).

TABLE 3
Drag coefficients for damping in still water

Case	β	$C_d K \sqrt{\beta}$	$\frac{C_d K \sqrt{\beta}}{26{\cdot}24}$
(1)	(2)	(3)	(4)
1	670 000	52·4	2·00
4	1 277 000	53·4	2·04

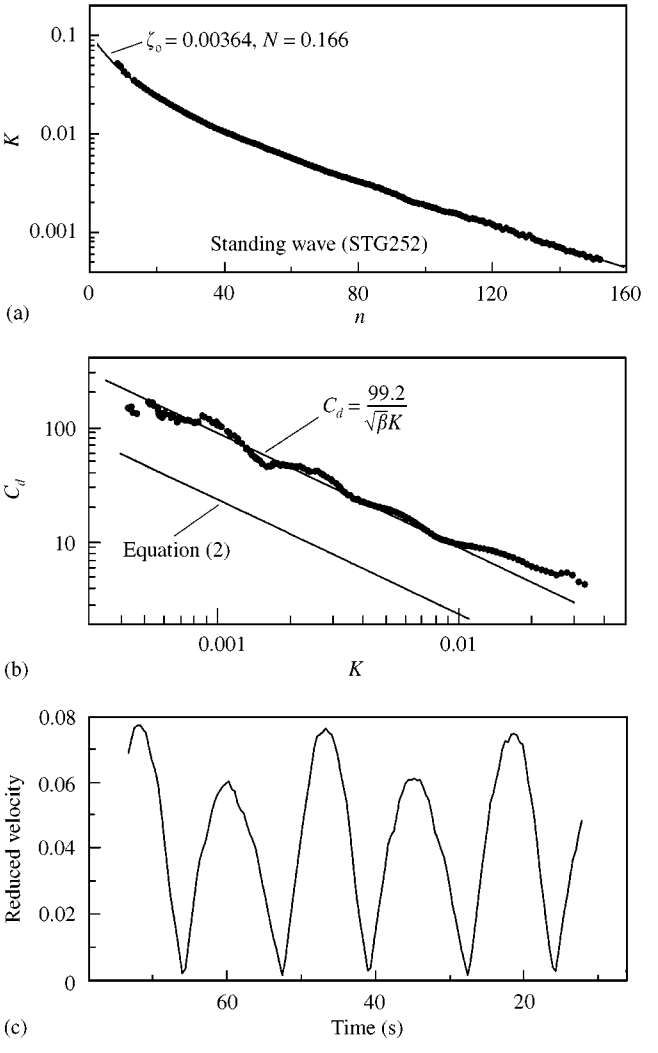

Figure 7. Measurements in a 25 s period standing wave: (a) the decaying amplitudes of successive oscillations fitted to equation (5) with the coefficients shown; (b) the drag coefficient, after corrections for structural and beam damping, as a function of K; (c) the instantaneous reduced velocity corresponding to the absolute horizontal velocity of the ambient flow. Keulegan–Carpenter numbers in (b) occurred at times indicated at the corresponding positions on the time axis in (c).

4.2. Measurements in Standing Waves

As mentioned above, no reliable data could be gathered while the carriage was moving, and instead measurements were made with the cylinder positioned at the node of standing waves of period 25 s. Figure 7 shows results for the case when the incident wave height was 0·4 m. Not surprisingly, the damping is influenced by the phase of the wave, but the measurements did not provide sufficient information for the instantaneous drag coefficients to be related reliably to the instantaneous flow. In Figure 8, averaged values of the product C_dK at small K are plotted against the absolute reduced velocity averaged over the duration of each test.

A quasi-steady approach to modelling the transverse force on an oscillating cylinder in a cross-flow is to assume that the overall force on the cylinder is proportional to the square of the speed of the instantaneous relative flow, and that it acts in the same direction. On this basis, the drag coefficient associated with the transverse component would be

$$C_dK = \frac{3\pi}{8} C_{dV} K \left\{ \cos \omega t \sqrt{\left(\frac{U_r}{K}\right)^2 + \cos^2 \omega t} \right\}, \tag{10}$$

taking only the amplitude of the fundamental frequency component of the expression in braces, where C_{dV} is the steady flow drag coefficient for the corresponding Reynolds number $\mathrm{Re} = Ud/\nu = \beta U_r$. When $U_r/K \gg 1$, equation (10) tends to

$$C_d K = \frac{3\pi}{8} C_{dV} U_r. \tag{11}$$

Besides equation (11) with $C_{dV} = 1$, three sets of data are shown in Figure 8: those at small K for $\beta = 166\,900$ from Chaplin & Subbiah (1998), and the present results at $\beta = 647\,000$ and 1 238 000. In the first of these, there appears to be a step change, which may indicate the conditions in which the effect of the current first penetrates the cylinder boundary layer. At higher β, however, the damping seems to increase continuously with U_r from its value in still

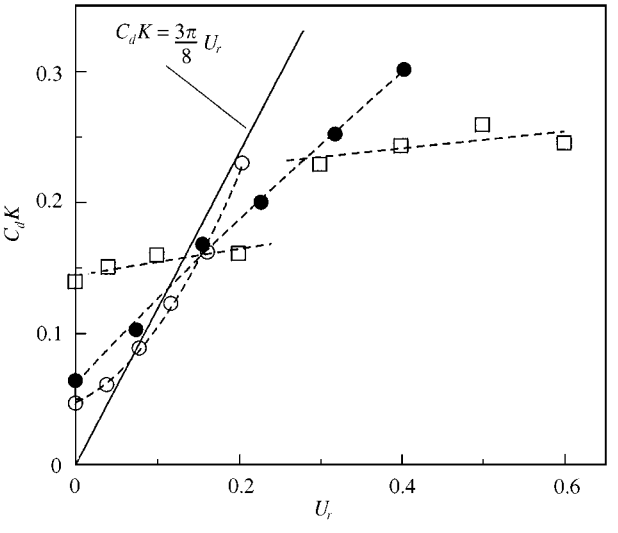

Figure 8. Drag coefficients in slowly varying and steady transverse currents. The present results at $\beta = 647\,000$ and 1 238 000 refer to measurements in which the cylinder was placed at the node of standing waves of period 25 s (33 times, and 63 times the cylinder frequency of oscillation respectively). Results at $\beta = 166\,900$ are from measurements in a steady current by Chaplin & Subbiah (1998). □, $\beta = 166\,900$; ●, $\beta = 647\,000$; ○, $\beta = 1\,238\,000$.

water. But if, as seems reasonable, the threshold reduced velocity depended on the Reynolds number, then it would appear at $U_r = 0{\cdot}064$ and $0{\cdot}034$ at $\beta = 647\,000$ and $1\,238\,000$, respectively. At such small current speeds, the effects of the current is likely to be weaker, and therefore much less obvious in these results.

The range of Reynolds numbers represented in Figure 8 covers those corresponding to critical conditions, and this probably accounts for the large change that is observed in the sensitivity of the measured damping to the reduced velocity. At $U_r = 0{\cdot}2$, Re increases from $33\,380$ at $\beta = 166\,900$ to $247\,600$ at $\beta = 1\,238\,000$. Over this interval, in which in steady conditions there are major alterations to the flow, there is a five-fold increase in the overall rate of change of C_dK with respect to U_r at constant β.

5. CONCLUSIONS

Measurements of the decaying oscillations of an elastically mounted cylinder in still water suggest that, at small amplitudes (below those linked with the onset of the Honji instability) at $\beta = 670\,000$ and $1\,277\,000$, the drag coefficient is twice that predicted by the Stokes–Wang laminar theory. This conclusion is in agreement with the results of earlier measurements at $\beta \approx 10^5$. Further work is needed to explain why the measurements do not agree with the theory, since, given the modest Reynolds numbers of the flow, it seems more likely that the discrepancy is caused by structural changes in the boundary layer, rather than by turbulence.

In a slowly varying transverse current the damping of the cylinder increased with the reduced velocity at a rate which appeared to depend on the mean Reynolds number of the current. At $\beta = 1\,238\,000$ and reduced velocities less than $0{\cdot}2$, the effect of the current was probably greater than that predicted by the quasi-steady relative velocity Morison equation, but at lower β the effect was much weaker.

Though the measurements described here were made at probably the highest value of β yet achieved in the laboratory, still there is a considerable gap between these and full-scale conditions.

ACKNOWLEDGEMENTS

Access to the Delta Flume was provided through the TMR programme of the European Comission. Funding for other elements of this work was provided by the EPSRC (contract GR/M10113). The assistance of Chris Retzler, Kesavan Subbiah, Nacho Zatarain and the staff of the Delta Flume is gratefully acknowledged.

REFERENCES

BEARMAN, P. W., DOWNIE, M. J., GRAHAM, J. M. R. & OBASJU, E. D. 1985 Forces on cylinders in viscous oscillatory flow at low Keulegan Carpenter numbers. *Journal of Fluid Mechanics* **154,** 337–356.

BEARMAN, P. W. & RUSSELL, M. P. 1996 Measurements of hydrodynamic damping of bluff bodies with application to the prediction of viscous damping of TLP hulls. In *Proceedings of the* 21*st Symposium of Naval Hydrodynamics*, Trondheim, Norway.

CHAPLIN, J. R. & SUBBIAH, K. 1998 Hydrodynamic damping of a cylinder in still water and in a transverse current. *Applied Ocean Research* **20,** 251–259.

HALL, P. 1984 On the stability of unsteady boundary layer on a cylinder oscillating transversely in a viscous fluid. *Journal of Fluid Mechanics* **146,** 337–367.

HONJI, H. 1981 Streaked flow around an oscillating circular cylinder. *Journal of Fluid Mechanics* **107,** 507–520.

LAZAN, B. J. 1968 *Damping of Materials and Members in Structural Mechanics*. Oxford: Pergamon Press.

OGILVIE, T. F. 1963 First- and second-order forces on a cylinder submerged under a free surface. *Journal of Fluid Mechanics* **16,** 451–472.

OTTER, A. 1990 Damping forces on a cylinder oscillating in a viscous fluid. *Applied Ocean Research* **12,** 153–155.

SARPKAYA, T. 1986 Force on a circular cylinder in viscous oscillatory flow at low Keulegan–Carpenter numbers. *Journal of Fluid Mechanics* **165,** 61–71.

STOKES, G. G. 1851 On the effect of the internal friction of fluids on the motion of pendulums. *Transactions of the Cambridge Philosophical society* **9,** 8–106.

TROESCH, A. W. & KIM, S. K. 1991 Hydrodynamic forces acting on cylinders oscillating at small amplitudes. *Journal of Fluids and Sructures* **5,** 113–126.

WANG, C.-Y. 1968 On high frequency oscillating viscous flows. *Journal of Fluid Mechanics* **32,** 55–68.

APPENDIX: SMALLER SCALE EXPERIMENTS TO TEST AN ALTERNATIVE ARRANGEMENT FOR END-PLATES

Experiments were carried out to test the idea of mounting the end-plates not on the oscillating cylinder, but, at a small offset, on the adjacent stationary framework. The importance of end-plates in this flow was demonstrated by Bearman & Russell (1996), who showed at ($\beta = 61\,000$) that, when the end-plates were only 1·25 times the cylinder diameter, large-scale vortex motion at the ends of the cylinder generated significant additional damping. This was eliminated when larger end-plates, of 2.25 times the cylinder diameter, were fitted.

The problem with end-plates that are attached to the cylinder is that they can give rise to significant additional oscillating forces. According to the solution by Stokes (1851) for the flow over a plate oscillating in its own plane in fluid otherwise unbounded and at rest, the component of shear stress on the plate in phase with its velocity V is $\rho V \sqrt{\omega\nu/2}$. Integrating this over the surfaces of two end-plates and comparing the result with the force on the cylinder predicted by equation (4), it follows that that the ratio of end-plate to cylinder damping at small K is theoretically

$$\frac{1}{4}\frac{(D/d)^2 - 1/2}{L/d} \tag{A.1}$$

where D and d are the endplate and cylinder diameters, and L is the cylinder length. This was found to be in reasonable agreement with the earlier measurements (Chaplin & Subbiah 1998). In the present case the ratio (A.1) was about 30% and, following Bearman & Russell, the end-plate damping could have been identified by repeating the tests with cylinders of different lengths (the "long–short" method). But at large scale this would have been rather costly, and it was desirable to find an alternative solution.

For this purpose, experiments were carried out in the 55 m flume at City University, with a smooth plastic cylinder of diameter 0·25 m and 1·4 m long, as a smaller scale trial before the Delta Flume tests.

The arrangement was basically similar. As shown in the sketches in Figure A.1, the cylinder was mounted at the ends of horizontal strain-gauged cantilever arms which were enclosed within submerged ducts. End-plates of 0·75 m diameter were attached to the supporting framework, parallel with the ends of the cylinder, at an adjustable offset. When submerged, with the ducts evacuated, the cylinder natural frequency was 1·93 Hz, implying $\beta = 112\,000$.

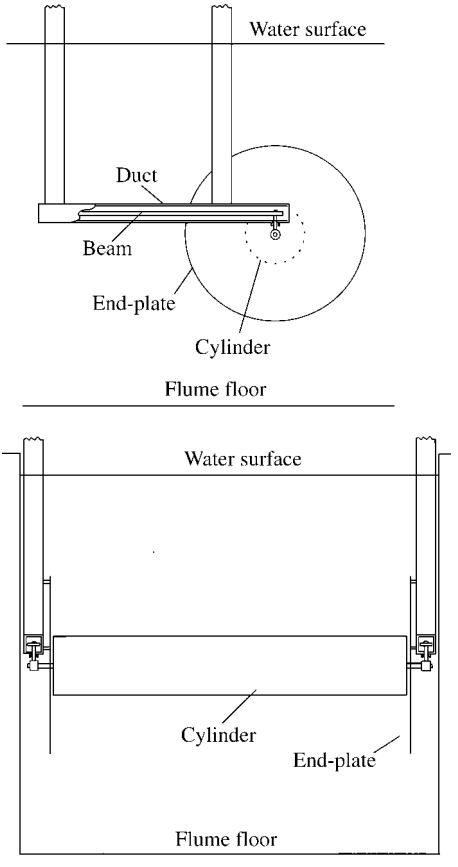

Figure A.1. Arrangements for the smaller scale tests, showing in the upper sketch the elevation, and in the lower sketch the cross-section, of the cylinder and support system. The cylinder was 0·25 m in diameter, 1·4 m long. The end-plates were attached to the support frame, and had slots to accommodate connections between the cylinder and the beams.

The results for different endplate gaps were compared after corrections had been made for the estimated oscillatory shear stresses on the plane ends of the cylinder. These can be estimated from the theory mentioned above, modified to include the effect of a second, stationary, plate that is parallel with the first. In this case the shear stress on the oscillating plate is

$$\rho V \sqrt{\omega\nu/2} \left[\frac{\sinh 2\alpha h + \sin 2\alpha h}{\cosh 2\alpha h - \cos 2\alpha h} \right], \tag{A.2}$$

where h is the width of the gap, and $\alpha = \sqrt{\omega/2\nu} = \sqrt{\pi\beta/d}$. As αh tends to infinity, the expression in brackets in (A.2) approaches unity; it is already within 1·5% of this limit when $\alpha h = 2{\cdot}4$.

In the small-scale tests the gaps h between the ends of the cylinder and the end-plates were set between 1 and 9 mm. But since αh was not less than 2·4 in any of the tests (at either scale), the correction (8) (about 2%) was applied to all of the data. In other words, theoretically it was not necessary to allow for the effect of the finite width of the gap on the shear stress on the ends of the cylinder.

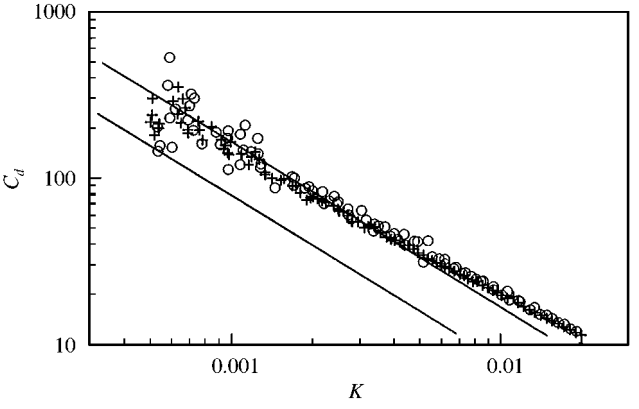

Figure A.2. Drag coefficients from tests to determine the effect of end-plate gaps, $\beta = 112\,000$. The lower line is the Stokes solution (2), and the upper line is the empirical formula (4). ○, End-plate gap = 1 mm; +, end-plate gap = 9 mm.

Results from the small-scale tests are shown in Figure A.2 for gap widths of 1 mm and 9 mm. The fact that they are in good agreement with each other, and with equation (4), which is based on earlier results, is taken as confirmation that direct measurements of damping on the cylinder can be made by this method.